

PAPER

Fabrication of a novel multi-sized and layered $(\text{Ti}_x, \text{Nb}_{1-x})\text{C}$ surface-reinforced layer on TiNb alloy

To cite this article: Jian-Lei Zhu *et al* 2019 *Mater. Res. Express* **6** 106512

View the [article online](#) for updates and enhancements.



IOP | ebooks™

Bringing you innovative digital publishing with leading voices to create your essential collection of books in STEM research.

Start exploring the **collection** - download the first chapter of every title for free.

Materials Research Express



PAPER

Fabrication of a novel multi-sized and layered $(\text{Ti}_x\text{Nb}_{1-x})\text{C}$ surface-reinforced layer on TiNb alloyJian-Lei Zhu^{1,2}, Li-Sheng Zhong^{1,2,4} , Yun-Hua Xu^{1,2,4}, Ji-Lin Li¹, Shao-Xiong Zhang¹ and Zheng-Xin Lu^{1,3}¹ School of Materials Science and Engineering, Xi'an University of Technology, Xi'an, 710048, People's Republic of China² International Research Center for Composite and Intelligent Manufacturing Technology, Xi'an University of Technology, Xi'an 710048, People's Republic of China³ Xi'an Zhitong Automation Technology Ltd Co., Xi'an 710048, People's Republic of China⁴ Authors to whom any correspondence should be addressed.E-mail: zhonglisheng@xaut.edu.cn and xuh_2000@126.com**Keywords:** diffusion, multi-sized, $(\text{Ti}_x\text{Nb}_{1-x})\text{C}$, structure**Abstract**

The multi-sized and layered $(\text{Ti}_x\text{Nb}_{1-x})\text{C}$ surface-reinforced layer (MLRL) was fabricated on the surface of the high temperature TiNb alloy via an *in situ* solid-phase diffusion reaction. The MLRL is formed by the diffusion of carbon atoms that diffuse from gray cast iron into the TiNb alloy. During the diffusion reaction, the MLRL is gradually formed *in situ* on the surface of the TiNb alloy. Thus, there is a good bonding interface between the MLRL and the substrate. Scanning electron microscope (SEM) analysis indicates that the MLRL is composed of three layers; the outer layer is micro-nano carbide particles, the middle layer is multi-sized carbide particles, and the inner layer is gradient micro-nano carbide particles. EDS results indicate that the different particles have different ratios of Ti/(Ti + Nb). The XRD results indicate that the MLRL is mainly composed of $(\text{Ti}_x\text{Nb}_{1-x})\text{C}$ particles; the diffraction peaks are located at 2θ positions between the corresponding peaks of TiC and NbC. Nanoindentation test results show that the hardness of the MLRL obviously increases (compared to that of TiC or NbC); the highest micro-hardness of the MLRL is nearly 2366 HV_{0.05}. Benefited from the solid-solution strengthening, the multi-sized and layered structures, the relationship between the strength and toughness of MLRL can be improved. Meanwhile the high hardness and volume fraction of $(\text{Ti}_x\text{Nb}_{1-x})\text{C}$ will obviously enhance the wear resistance of the reinforced layer.

1. Introduction

Carbide-reinforced metal matrix composites (CRMMC) possess the characteristics of outstanding hardness, high wear resistance, a matrix with excellent toughness, and economic benefits [1–3]; Thus CRMMC have been widely studied and applied. Among many preparation technologies that have been used for metal matrix composites. Such as powder metallurgy, extrusion casting, casting infiltration molding and laser cladding. The combination of preparation technologies with *in situ* technology can obtain a cleaner and more stable interface between the matrix and the reinforced phases [4, 5]. Therefore, the *in situ* synthesis has been widely studied and applied. Our team has been conducting a long-term investigation on the surficial reinforcement of metal produced by *in situ* solid-phase diffusion reaction. The *in situ* reaction happens in the solid-phase, and therefore, the formed reinforcements have a higher volume fraction and smaller particle size, which provide improved properties.

A series of carbide cermet that contain the reinforcements of TiC [6], NbC [7], TaC [8], VC [9], WC [10], and Mo₂C [11], have been produced via *in situ* solid-phase diffusion reactions. All of the carbide cermets have a good binding interface and high hardness. However, the contradictory relationship between strength and toughness has impeded the popularization of cermet. The toughness decreases obviously with the increase in strength. Therefore, overcoming this contradictory relationship is a challenge that researchers must to confront. This problem has created a bottleneck that inhibits further improvement to matching strength and toughness

through the use of single-phase carbides, whereas multiple-phase carbides provide a new path to obtaining improved properties [12, 13].

On the basis of strong carbide formation characteristics of Ti and Nb, the different particle sizes and the different growth mechanisms (previous studies have indicated that the sizes of the TiC particles range from hundreds of nanometers to tens of microns [6], whereas the sizes of NbC particles are hundreds of nanometers [7]), metal matrix surface-reinforced layer composites reinforced with the carbide of $(\text{Ti}_x\text{Nb}_{1-x})\text{C}$ were designed in this work. In the composite, the $(\text{Ti}_x\text{Nb}_{1-x})\text{C}$ particles have different sizes and morphology. Compared with previously cermet reinforced layer, the $(\text{Ti}_x\text{Nb}_{1-x})\text{C}$ MLRL still have good bonding interfaces, high volume fraction of surface carbides, and good comprehensive properties [6, 7]. Meantime, the multi-layered microstructure, that is composed of different particles and multiple elements (Ti and Nb), will simultaneously improve the toughness and increase the strength. In terms of microstructure toughening, multi-layered microstructures that consist of different sized particles can influence the crack propagation pattern and prolong the crack path, realize the objective of microstructure toughening [14]. In terms of solution strengthening, first-principles calculation results of $(\text{TiNb})\text{C}$ [15] indicate that replacing of Ti with Nb atoms in TiC will further improve the calculated hardness, which obviously higher than the values of TiC (25.78 GPa) and NbC (22.69 GPa); the highest hardness is as high as 29 GPa. This proves that $(\text{Ti}_x\text{Nb}_{1-x})\text{C}$ provides higher hardness in theory.

Therefore, a combination of the different growth characteristics of TiC and NbC, *in situ* solid-phase diffusion reaction technology is adopted to process the MLRL on the surface of high temperature TiNb alloys. In this work, a novel MLRL was prepared via *in situ* reaction. This MLRL has many outstanding properties, including high temperature stability, high hardness, and high wear resistance. Additionally, compared with TiC and NbC surface-reinforced layer, the multi-sized and layered microstructure of the MLRL improves the toughness; the solid-solution strengthening effect provides higher hardness. Therefore, this investigation of the MLRL is necessary and interesting. The composition of carbide particles, phases, sizes and the distribution of the MLRL were investigated in this paper.

2. Experimental procedures

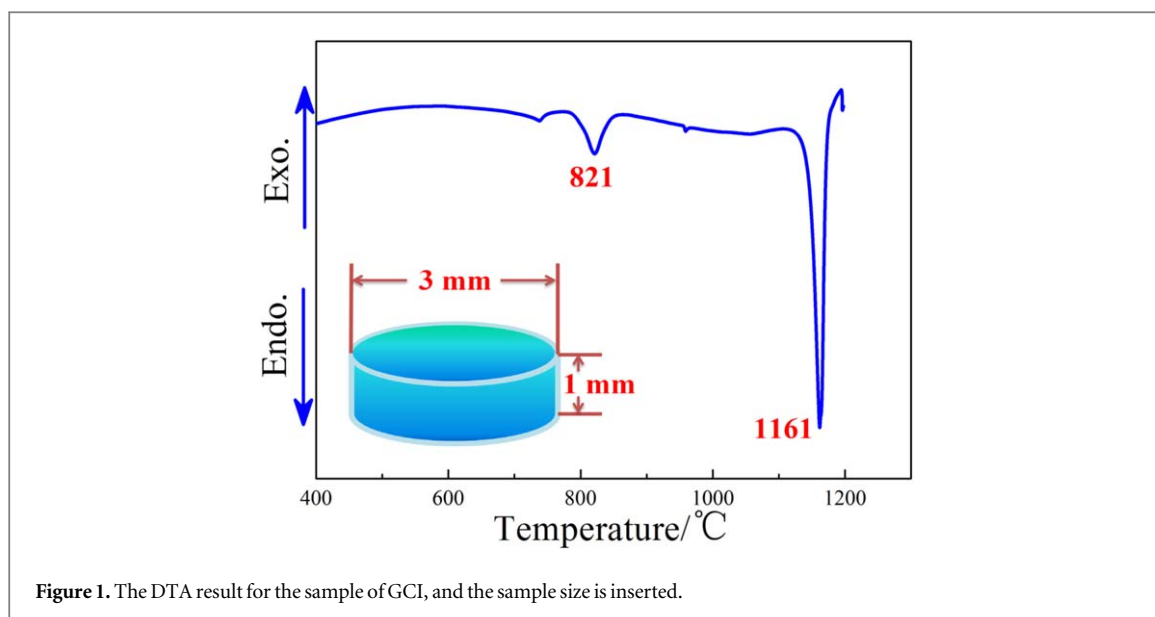
2.1. Raw materials and preparation

A high temperature TiNb alloy (43.95 wt% Nb, 53.36 wt% Ti, 0.67 wt% C, 2.0 wt% Si, a small amount of Fe) was used as the substrate with dimensions of $10 \times 10 \times 2$ mm. The gray cast iron (GCI) (3.25 wt% C, 2.38 wt% Si, 0.56 wt% Mn, 0.014 wt% S, and balance Fe) made by casting was chosen as the 'carbon donor' with dimensions of $10 \times 10 \times 1$ mm. The NbTi sheet (substrate) and GCI sheet was polished and ultrasonically cleaned in nitric acid solution and acetone for several minutes, respectively. The couple of the substrate and CGI sheet were contacted together on the ways of face to face and coated with graphite paper. Finally the precursors were made well. After that, the produced precursors were put into the horizontal tube furnace under Ar gas atmosphere with a flow rate of 5 ml min^{-1} .

Figure 1 shows the differential scanning calorimeter (DSC) curve and the schematic illustrations of the sample via differential thermal analysis (DTA), the endothermic peak at 1161°C . The GCI is hypoeutectic iron with a carbon content of 3.25 wt%. Because of the influence of Si, Mn, Ti and Nb in precursor, the endothermic peak is the expression of the eutectic reactions of $\text{L} + \gamma \rightarrow \text{Fe}_3\text{C} + \gamma + \text{L}_\text{d}$, and the 1161°C is the eutectic temperature. The *in situ* solid-phase diffusion reaction depends on the C atoms diffusing into NbTi. But the diffusion rates of C atoms are mainly influenced by temperature. Therefore, high diffusion rate of C atoms can be gained by increasing the temperature as much as possible on the premise that there is no liquid phase generated in the precursors. According to this reason, the temperature of the *in situ* solid-phase diffusion reaction is set at 1150°C . The heat treatment process is 1150°C for 4 h, then cooling to 1050°C for 4 h, thirdly cooling to 700°C for 1 h, lastly cooling to room temperature in the furnace.

2.2. Characterization

The prepared samples were cut into two parts with wire-electrode cutting, and the cross-section of one part was polished for cross-sectional microstructural analysis. Separated the GCI sheet from another part via mechanical easily, and the appeared surface of MLRL was polished for the surficial microstructural analysis. The microstructures, the chemical components were characterized by scanning electron microscope (SEM, JSM-6700F, JEOL) equipped with an energy dispersive spectral (EDS-Oxford, INCA) analyzer. The field emission transmission electron microscope (TEM, JEM-3010) was used to analyze the morphology features and the crystal structure with selected area electron diffraction (SAED) patterns. The phase component of the specimen was identified on x-ray diffractometer (XRD, Smart Lab) with $\text{Cu K}\alpha$ radiation at 40 kV and 200 mA in the 2θ of 30° – 90° . The micro-hardness was tested on a Vickers indenter (Tukon2100); the test was carried out on the



polished surface with a load of 0.05 kg, 0.10 kg and 0.5 kg, respectively. The hardness and Young's modulus was tested on G200 nanoindentation tester (Agilent technologies) with a Berkovich indenter. The test was carried out on the polished cross-section with a load of 400 mN.

3. Results

The cross-section and polished surface of reinforced layers are characterized using SEM, and the corresponding microstructures are shown in figures 2 and 3, respectively. The MLRL is formed by diffusion of C atoms from gray cast iron (GCI) into βTiNb , and the *in situ* reaction of $\text{C} + \beta\text{TiNb} \rightarrow (\text{Ti}_x\text{Nb}_{1-x})\text{C}$ occurs on the surface of the TiNb alloy. Therefore the MLRL generated *in situ* on the surface of the TiNb alloy. Also, the cross-sectional image (figure 2(a)) reveals that there is a good interface between the substrate and the MLRL. EDS line scan results show obvious changes in the Fe, Ti and Nb content at the interface. Compared with compositions of the substrate, the linear distribution of the elements reveals that the diffusion distance of Fe atoms is very limited in MLRL, but the ratios of $\text{Ti}/(\text{Ti} + \text{Nb})$ change obviously. This phenomenon indicates that Ti and Nb redistribute during the formation of the MLRL. The figure 2(b) shows that the MLRL is mainly made up of three layers. The outer layer is composed of submicro-sized carbide particles (SMCP) and the thickness of this layer is less than $2\text{ }\mu\text{m}$. Figures 2(c) and (d) show the microstructures of the upper and inner interfaces of the MLRL, respectively. The middle layer is composed of multi-sized mixed carbide particles, which are composed of micro and nano-sized carbide particles (MNCP) (light gray region) and micro-sized carbide particles (MCP) (dark gray region). The inner layer is composed of gradient and submicro-sized carbide particles (GSMCP).

The polished surface shows the microstructure of the middle layer (figure 3). The deeply etched results indicate that the MNCP are surrounded by MCP (figure 3(a)). Furthermore, in the middle layer, the volume ratio of MCP increases gradually as the distance to the inner side decrease. From the mapping results (figure 3(c)), it is found that the dark gray region is Ti rich, whereas the light gray region is Nb rich. Table 1 shows EDS results of points in 1, 2, 3 and 4, which are marked in figures 2(c) and (d). The results at the points 1 and 2 indicate that both the MCP (dark gray areas) and MNCP (light gray areas) are mainly composed of C, Ti, Nb and a small amount of Fe. The ratio of $\text{Ti}/(\text{Ti} + \text{Nb})$ in light gray areas is about 0.74 and about 0.86 in the dark gray areas. Combined with line scan analysis results, these observations demonstrate that a redistribution of Ti and Nb atoms occurs during the formation of MLRL. The final Ti rich and Nb rich carbides have different morphologies and different components.

Further study of the $(\text{Ti}_x\text{Nb}_{1-x})\text{C}$ particles was carried out using TEM to characterize the microstructure and the crystal structure. Figure 4(a) shows the morphology of the submicro-sized particles; the particles are equiaxed. SAED pattern results are shown in figure 4(b) and indicate that the particle has a face center cubic (fcc) crystal structure with a crystal zone axis of $B = [011]$. Figure 4(c) shows the morphology of the micro-sized particles; the particles are columnar; the SAED pattern (figure 4(d)) indicates that the micro-sized particles has a fcc crystal structure with a crystal zone axis of $B = [\bar{1}11]$. Combined with the EDS analysis, it is confirmed that the submicro-sized and micro-sized particles are both $(\text{Ti}_x\text{Nb}_{1-x})\text{C}$ and have a fcc crystal structure.

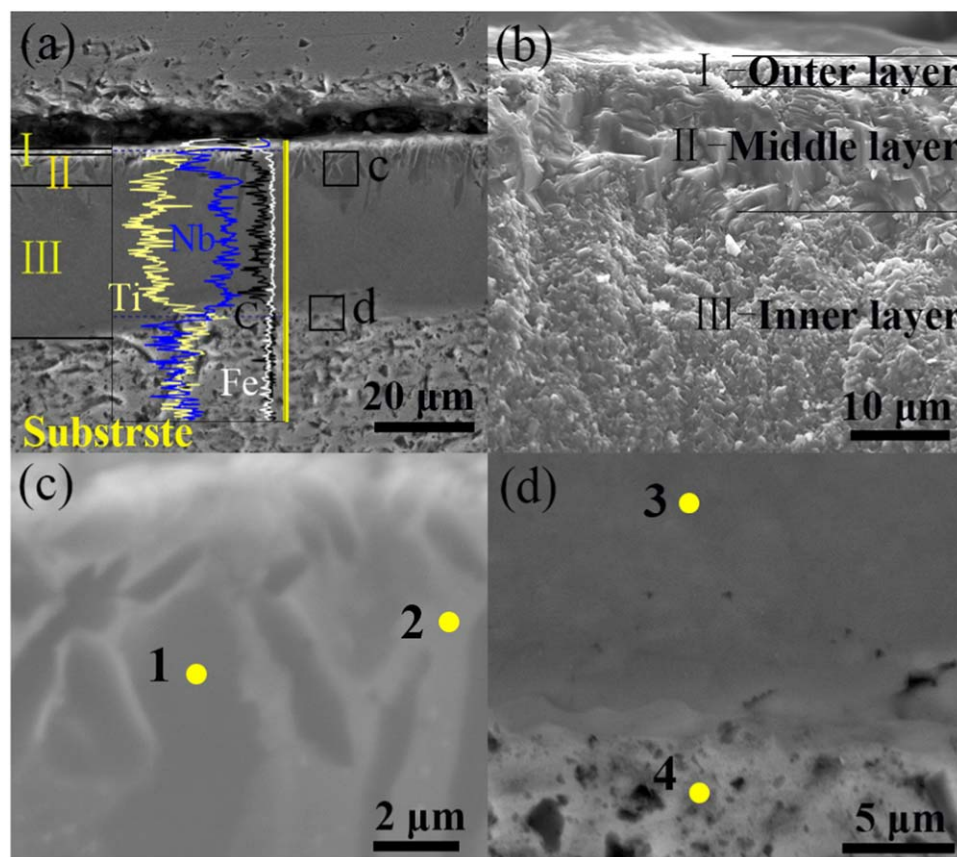


Figure 2. (a) Cross-sectional image. The EDS line scan result is included, and the intensity of C is amplified by a factor of 3 for clarity. (b) Cross-sectional image after brittle fracture. (c) and (d) Local magnified images of the boxes marked in (a).

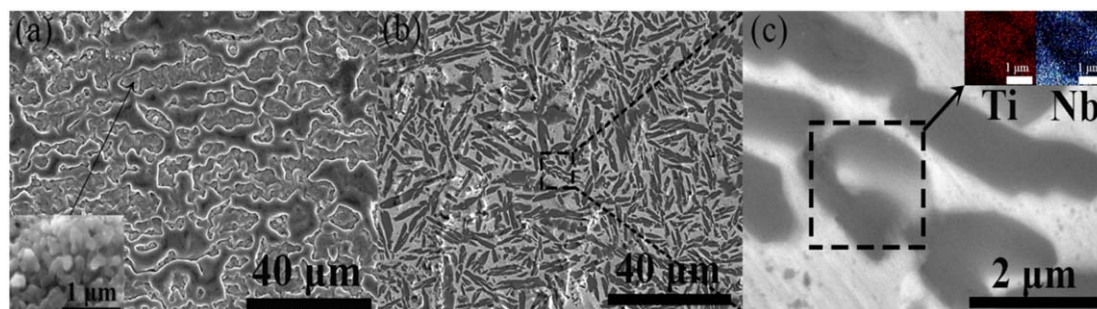


Figure 3. SEM image of deeply etched surface (a) and polished surface (b) of the middle layer. (c) Magnified image with EDS mapping results of Ti and Nb insert in the upper-right corner.

Table 1. Chemical composition of points 1, 2, 3, 4 marked in figures 2(c) and (d), at%.

Elements	C	Ti	Nb	Fe	Si	$x = \text{Ti}/(\text{Ti} + \text{Nb})$
1	55.75	37.39	6.27	0.59	—	0.86
2	60.63	28.75	9.97	0.62	—	0.74
3	57.34	32.41	10.25	—	—	0.76
4	27.05	44.16	20.44	2.56	5.78	0.68

Furthermore, XRD was used to identify the phases in the MLRL, and the results are shown in figure 5. The blue line shows an obvious double peak phenomenon, whereas red line is not obvious; there are only small peaks at the sides of the peaks. In spite of that, all of the peaks lie between the 2θ positions of NbC and TiC. The double

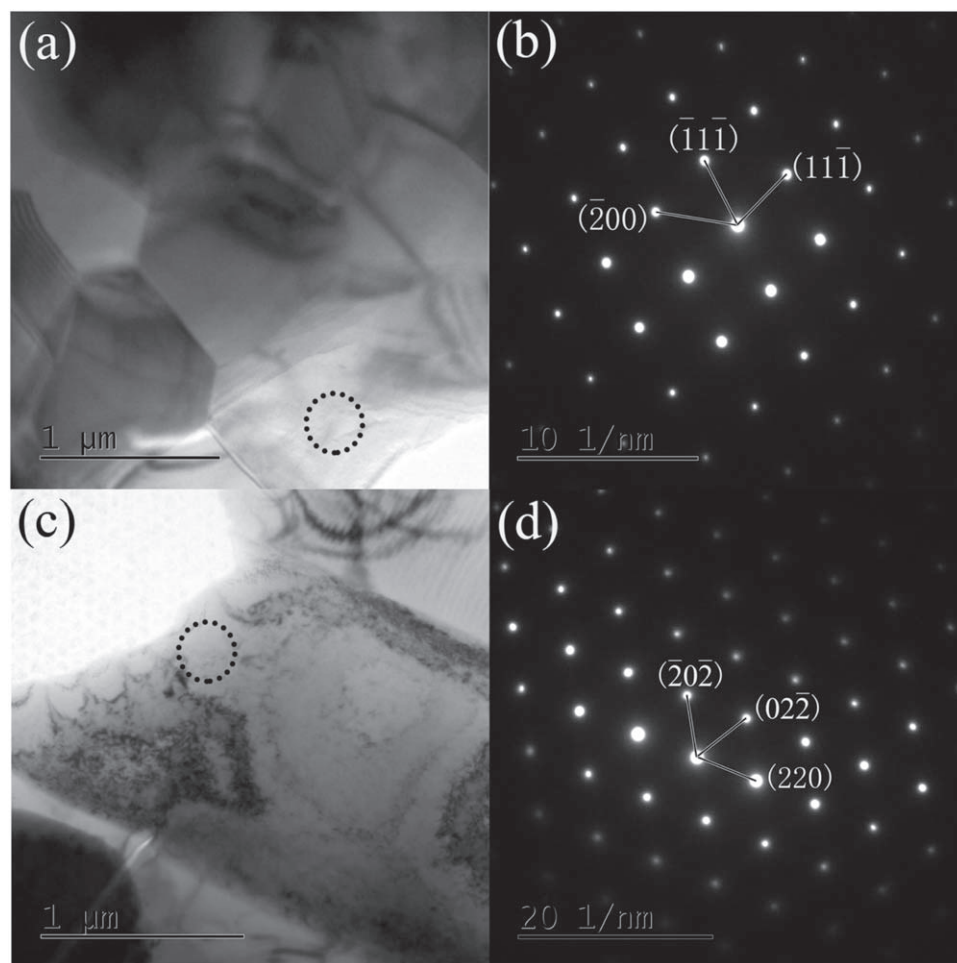


Figure 4. TEM image and selected area electron diffraction (SAED) pattern of the $(\text{Ti}_x\text{Nb}_{1-x})\text{C}$ particles. TEM image (a) and SAED pattern (b) of the submicro-sized particles; TEM image (c) and SAED pattern (d) of the micro-sized particles.

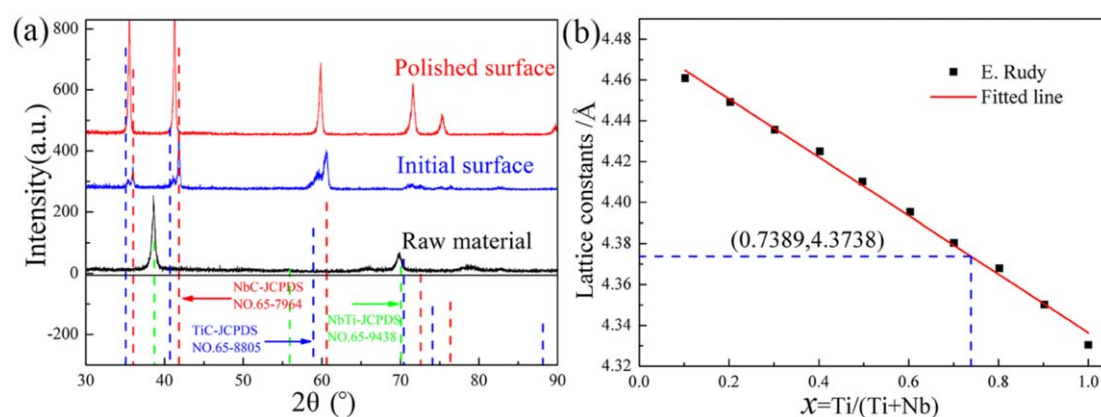


Figure 5. (a) XRD results of the different layers of the MLRL and substrate, and the initial surface obtained by splitting off the GCI and without any polishing. (b) Relationship between ratio of $\text{Ti}/(\text{Ti} + \text{Nb})$ and lattice constants.

peak phenomena in the XRD result for the initial surface indicate that a redistribution of Ti and Nb atoms obviously occurred, and that two different phases formed in the outer layer.

The essential reason for the appearance of double peaks is that the exchange of Ti and Nb in $(\text{Ti}_x\text{Nb}_{1-x})\text{C}$ results in different amounts of lattice distortion. Own to the different of lattice constant of NbC and TiC, with changes in the $\text{Ti}/(\text{Ti} + \text{Nb})$ ratio, the diffraction peaks of $(\text{Ti}_x\text{Nb}_{1-x})\text{C}$ will change between the peaks of NbC and TiC. Therefore, the phases in the surficial reinforced layer are different $(\text{Ti}_x\text{Nb}_{1-x})\text{C}$ and the outside surface

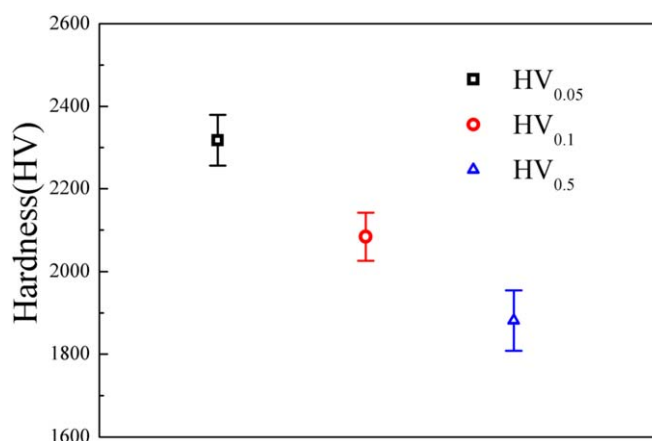


Figure 6. Micro-hardness results of the polished surface of the MLRL with loads of 0.05 kg, 0.10 kg and 0.5 kg.

are obviously more different. According to the XRD peak values, the 2θ value of the highest peak is 35.52. On the basis of the 2θ value of the highest peak, the lattice constant of the main phase can be calculated using equations (1) and (2) for a cubic crystal system; the lattice constant of the main phase is 4.3738 Å. Relevant research results have proven that the lattice constants of $(\text{Ti}_x\text{Nb}_{1-x})\text{C}$ are approximately linearly distributed with the exchange of Ti and Nb; therefore, in combination with the research results of Rudy [16], our results (figure 5(b)) confirm that x corresponds to the main phase with a lattice constant of 4.3738 Å and that the values of x is 0.7389. However, there are some secondary peaks beside the largest peak, the appearance of secondary peaks are caused by the exchange of Ti and Nb in $(\text{Ti}_x\text{Nb}_{1-x})\text{C}$, and this is the reason for the different values of x , which are distributed around 0.7389.

$$2d \sin \theta = \lambda \quad (1)$$

$$\frac{1}{d^2} = \frac{h^2 + k^2 + l^2}{a^2} \quad (2)$$

Micro-hardness testing on the surface of MLRL was carried out by using a Vicker's indenter with different loads. The highest surface micro-hardness of the MLRL is 2366 HV_{0.05}, and this value is dependent on the loads (figure 6). Also, a nanoindentation test on the cross-section of the MLRL was conducted using a Berkovich indenter with a load of 400 mN. The hardness is as high as 32.06 GPa, and the elastic modulus is as high as 467.07 GPa. In conclusion, the hardness of the MLRL is significantly improved. Also, the hardness of the $(\text{Ti}_x\text{Nb}_{1-x})\text{C}$ MLRL is obviously higher than the values of TiC (27.7 GPa) and the NbC (23.5 GPa) cermet [6, 7], which were prepared using the same process.

4. Discussion

In the Ti-Nb-Fe-C diffusion system, Ti, Nb and Fe atoms mainly adopt a vacancy diffusion mechanism. In contrast, C atoms have a double-diffusion mechanism, that is, a vacancy diffusion mechanism and an interstitial diffusion mechanism. However, the main style is interstitial diffusion mechanism. Because of the different diffusion mechanism of C atoms, the diffusion rate of C in the $(\text{Ti}_x\text{Nb}_{1-x})\text{C}$ MLRL is four orders of magnitude higher than those of Ti, Nb and Fe [17]. Thus, the growth of the $(\text{Ti}_x\text{Nb}_{1-x})\text{C}$ MLRL is controlled by the diffusion rate of C atoms that diffuse through the surface-reinforced layer from GCI into TiNb side. Because of the huge difference in the diffusion rates, the Ti, Nb and Fe atoms do not diffuse over a long range. Therefore, only a small amount of Fe atoms diffuse into the outside layer and this is confirmed by the EDS line scan results.

From the above analysis, it is concluded that Fe atoms have a small influence on the reaction of the whole system and the diffusion of Fe is limited to a local range. Accordingly, the reaction system can be simplified to the Ti-Nb-C system. Driven by a concentration gradient, the C atoms in GCI diffuse into the β -TiNb solid solution and react with Ti and Nb to form $(\text{Ti}_x\text{Nb}_{1-x})\text{C}$. In the reaction process of $\text{C} + \text{TiNb} \rightarrow (\text{Ti}_x\text{Nb}_{1-x})\text{C}$, C atoms react with Ti atoms and Nb atoms, and the Gibbs free energy of $\text{Ti} + \text{C} \rightarrow \text{TiC}$ and $\text{Nb} + \text{C} \rightarrow \text{NbC}$ are ΔG_{TiC} and ΔG_{NbC} , respectively. The conclusion that $\Delta G_{\text{TiC}} < \Delta G_{\text{NbC}}$ at temperatures of 900 °C–1300 °C has been confirmed [18]. Therefore, C atoms have a greater affinity to Ti atoms than to Nb atoms. Because of differences in free energy and chemical potential, the Ti and Nb atoms in the formed $(\text{Ti}_x\text{Nb}_{1-x})\text{C}$ diffuse at short distances, Ti atoms trend to become enrich, and then Ti-rich carbides formed. As the reaction proceeds, the thickness of the reinforced layer gradually increases, in the meantime, the thicker reinforced layer acts as an obstacle to slow

the diffusion of C atoms. Therefore, with the thickening of the MLRL, resistance to the diffusion of C atoms becomes more obvious. Ti and Nb atoms have a certain amount of time to become redistributed. In the inner layer, Ti and Nb react with a certain amount of C and generate $(\text{Ti}_x\text{Nb}_{1-x})\text{C}$. EDS results of point 3 in figure 2 indicate that the value of x for $\text{Ti}/(\text{Ti} + \text{Nb})$ is 0.76; compared with the raw materials, Nb atoms at point 3 (figure 2) are superfluous. Therefore the surplus of Nb atoms moves along the same direction as the diffusion direction of C atoms. The final phenomenon is that the Nb content in the inner layer is lower than that in the raw materials, but the Nb content in the vicinity of point 4 (figure 2) is higher than that in the raw materials. With the thickening of the reinforced layer, the diffusion rate of C atoms decreases gradually, and this means that there is a decrease in free C atoms. Along with the decrease of free C atoms, the nucleation rate of $(\text{Ti}_x\text{Nb}_{1-x})\text{C}$ decreases gradually. Therefore, the size of the particles increases. A gradient microstructure of the inner layer occurs, consisting of different particles that increase in size. This gradient microstructure improves the interfacial structure and the toughness [19].

Utilizing this special diffusion, accumulation and growth mechanism, a layered microstructure with multi-sized mixed particles on the middle layer and a gradient of micro-nano-sized particles on the inner layer are prepared. In the middle layer of MLRL, particles that are hundreds of nanometers and tens of microns constitute a multi-sized mixed structure. A multi-sized mixed and layered microstructure changes the crack propagation path and then achieves the effect of microstructure toughening [14]. Submicro-sized particles in the inner side play a fine-grain strengthening role, and provide high strength and high toughness. The exchange of Ti and Nb play a role of solid-solution strengthening. Compared with the reinforced layers of TiC (27.7 GPa) [6] or NbC (23.5 GPa) [7] formed via the same process, the MLRL has higher hardness; specifically, the hardness is as high as 32.06 GPa. Generally speaking, the MLRL is strengthened by the solid solution via the exchange of Ti and Nb [15] and toughened by the multi-sized mixed and layered gradient structure.

5. Conclusions

A novel multi-sized and layered $(\text{Ti}_x\text{Nb}_{1-x})\text{C}$ surface-reinforced layer was fabricated via *in situ* solid-phase diffusion reaction. The MLRL is composed of three layers; the middle layer of MLRL consists of multi-sized particles, in which the micro-sized particles (dark gray) are Ti rich, whilst the nano-sized particles (light gray) are Nb rich. The gradient inner layer consists of micro-nano sized particles. The multi-sized mixed and layered gradient structures change the crack propagation pattern and prolong the crack path, achieving the toughening effect.

The different chemical properties of Ti and Nb cause the formation of different $(\text{Ti}_x\text{Nb}_{1-x})\text{C}$; and the x values distribute around 0.7389. The hardness of the MLRL is improved via the exchange of Ti and Nb in the $(\text{Ti}_x\text{Nb}_{1-x})\text{C}$.

The $(\text{Ti}_x\text{Nb}_{1-x})\text{C}$ provide higher hardness and elastic modulus value, that is as high as 32.06 GPa and 467.07 GPa, and the surficial micro-hardness of the MLRL is as high as 2366 HV_{0.05}.

The layered structures, multi-sized mixed particles, gradient structures and solid solution strength interact together, all of those act positive roles in the strengthening and toughening of the MLRL.

Acknowledgments

This work was supported by the Key-point Research and Invention Program of Shaanxi Province [Grant No. 2017ZDXM-GY-043], and the International Research Center for Composite and Intelligent Manufacturing Technology [Grant No. 2018GHJD-17].

ORCID iDs

Li-Sheng Zhong  <https://orcid.org/0000-0002-3315-0043>

References

- [1] He X, Song R G and Kong D J 2019 Effects of TiC on the microstructure and properties of TiC/TiAl composite coating prepared by laser cladding *Optics & Laser Technology* **112** 339–48
- [2] Wang X H, Zou Z D, Qu S Y and Song S L 2005 Microstructure and wear properties of Fe-based hardfacing coating reinforced by TiC particles *J. Mater. Process. Technol.* **168** 89–94
- [3] Cao Y-B, Zhi S-X, Gao Q, Tian X-T, Geng T, Guan X and Qin C 2016 Formation behavior of *in situ* NbC in Fe-based laser cladding coatings *Mater. Charact.* **119** 159–65
- [4] Berns H and Wewers B 2001 Development of an abrasion resistant steel composite with *in situ* TiC particles *Wear* **251** 1386–95

- [5] Yang L, Yu T, Li M, Zhao Y and Sun J 2018 Microstructure and wear resistance of *in situ* synthesized Ti(C, N) ceramic reinforced Fe-based coating by laser cladding *Ceram. Int.* **44** 22538–48
- [6] Zhu J, Zhong L, Xu Y, Cai X, Bai F, Ding Y, Lu Z and Wu H 2018 Characterization and formation mechanisms of the TiC-Fe cermet layer in Ti-TiC-Fe composites *Vacuum* **155** 631–6
- [7] Zhao N, Xu Y, Zhang W, Zhao Z, Zhong L and Fu Y 2016 Gradually varying mechanical properties of *in situ* synthesized NbC-Fe-graded composite coating *Mater. Sci. Technol.* **33** 220–6
- [8] Zhao N, Xu Y, Zhong L, Yan Y, Song K, Shen L and Ovcharenko V E 2015 Fabrication, microstructure and abrasive wear characteristics of an *in situ* tantalum carbide ceramic gradient composite *Ceram. Int.* **41** 12950–7
- [9] Cai X, Zhong L, Xu Y, Lu Z, Li J, Zhu J, Ding Y and Yan H 2018 Microstructural characterization of a V2C and V8C7 ceramic-reinforced Fe substrate surface compound layer by EBSD and TEM *J. Alloys Compd.* **747** 8–20
- [10] Cai X, Zhong L, Xu Y, Li X and Liu M 2019 Microstructure and fracture toughness of a WC-Fe cemented carbide layer produced by a diffusion-controlled reaction *Surf. Coat. Technol.* **357** 784–93
- [11] Zhao Z, Hui P, Wang T, Xu Y, Zhong L, Zhao M, Yang D and Wei R 2018 Fabrication of Mo2C coating on molybdenum by contact solid carburization *Appl. Surf. Sci.* **462** 48–54
- [12] Jang J H, Lee C-H, Heo Y-U and Suh D-W 2012 Stability of (Ti,M)C (M = Nb, V, Mo and W) carbide in steels using first-principles calculations *Acta Mater.* **60** 208–17
- [13] Wen H K, Bhatia V, Dolman K, Lucey T, Tang X, Li C, Proust G and Cairney J 2017 A study on novel AISI 304 stainless steel matrix composites reinforced with (Nb_{0.75}, Ti_{0.25})C *Wear* **398–399** S004316481731178X
- [14] Bouville F, Maire E, Meille S, Van de Moortele B, Stevenson A J and Deville S 2014 Strong, tough and stiff bioinspired ceramics from brittle constituents *Nat. Mater.* **13** 508–14
- [15] Zhao C, Zhou Y, Xing X, Sha L, Ren X and Yang Q 2018 Precipitation stability and micro-property of (Nb, Ti)C carbides in MMC coating *Journal of Alloys & Compounds* **763** 670–8
- [16] Rudy E Phase equilibria investigation of binary, ternary, and higher order systems: I. The phase diagrams of the systems Ti-Nb-C, Ti-Ta-C, and Ti-Mo-C[M]. Technical report AFML-TR-69-117:I. August 1970. Air force materials laboratory air force systems command wright-patterson air force base, Ohio
- [17] Sarian S 1969 Diffusion of 44Ti in TiCx *J. Appl. Phys.* **40** 3515–20
- [18] Li Q, Lei Y and Fu H 2014 Growth mechanism, distribution characteristics and reinforcing behavior of (Ti, Nb)C particle in laser clad Fe-based composite coating *Appl. Surf. Sci.* **316** 610–6
- [19] Bian X, Yuan F, Zhu Y and Wu X 2017 Gradient structure produces superior dynamic shear properties *Materials Research Letters* **5** 501–7